Bulletin of Mathematical Biology (2009) 71: 602–626
DOI 10.1007/s11538-008-9373-7

ORIGINAL ARTICLE

An "Age"-Structured Model of Hematopoietic Stem Cell Organization with Application to Chronic Myeloid Leukemia

Ingo Roeder[a,b,*], Maria Herberg[a], Matthias Horn[a]

[a] *Institute for Medical Informatics, Statistics and Epidemiology, University of Leipzig, Leipzig, Germany*
[b] *Department of Computing, Goldsmiths, University of London, London, UK*

Received: 17 March 2008 / Accepted: 18 November 2008 / Published online: 20 December 2008

Abstract Previously, we have modeled hematopoietic stem cell organization by a stochastic, single cell-based approach. Applications to different experimental systems demonstrated that this model consistently explains a broad variety of *in vivo* and *in vitro* data. A major advantage of the agent-based model (ABM) is the representation of heterogeneity within the hematopoietic stem cell population. However, this advantage comes at the price of time-consuming simulations if the systems become large. One example in this respect is the modeling of disease and treatment dynamics in patients with chronic myeloid leukemia (CML), where the realistic number of individual cells to be considered exceeds 10^6. To overcome this deficiency, without losing the representation of the inherent heterogeneity of the stem cell population, we here propose to approximate the ABM by a system of partial differential equations (PDEs). The major benefit of such an approach is its independence from the size of the system. Although this mean field approach includes a number of simplifying assumptions compared to the ABM, it retains the key structure of the model including the "age"-structure of stem cells. We show that the PDE model qualitatively and quantitatively reproduces the results of the agent-based approach.

Keywords Chronic myeloid leukemia · Imatinib · Hematopoietic stem cell · Mathematical model · Partial differential equation · Computer simulation

1. Introduction

We previously proposed to explain hematopoietic stem cell (HSC) organization as a self-organizing process within a heterogeneous population of individual cells interacting with each other and with their microenvironment (Loeffler and Roeder, 2002; Glauche et al., 2007). As an essential feature of such a concept, we proposed the interaction rules to be dependent on the actual state of individual cells and on the signals they are receiving from

*Corresponding author.
E-mail address: ingo.roeder@imise.uni-leipzig.de (Ingo Roeder).

their microenvironmental context. Particularly, the latter assumption implies that even identical cells (i.e., cells with equal functional potential) can behave differently, depending on the actual context they are exposed to.

To facilitate simulation analyses of this general concept, we formulated a mathematical model (Roeder and Loeffler, 2002; Roeder, 2003) within an agent-based framework (d'Inverno and Luck, 2004). In this single cell-based approach, stem cells are assumed to reside in two different signaling contexts, denoted as A and Ω. Individual cells are able to change the context with a probability that depends on the actual number of cells within these two signaling contexts and on the actual state of the particular cell. In contrast to this dynamically regulated but stochastic transition process, the development of cells within the two contexts is considered to follow fixed deterministic rules. Particularly, we assume that cells within context Ω are actively proliferating, whereas cells in A are considered to be quiescent, i.e., arrested in a nonproliferating state denoted as G_0. Moreover, we assume the cell-intrinsic variable a, which determines the affinity of a cell for residing in context A, to develop differently depending on the actual context of the cell. Whereas a gradually decreases for cells in Ω, it increases (up to a maximum value $a_{\max}$) for cells in A. Cells with $a < a_{\min}$ are unable to move into A (and, therefore, to regenerate a) and must remain in Ω. They are denoted as differentiated cells.

These rules imply the existence of two "age"-structured subpopulations of HSCs with respect to the context affinity a. However, in contrast to normal age, the context affinity a can reversibly change within the interval $[a_{\min}, a_{\max}]$. Due to the particular structure of the model, which relates residence in A to cell cycle dormancy and to regeneration of a, context affinity a also characterizes the potential of HSCs with respect to their repopulation potential and can, therefore, be interpreted as a measure of stem cell potential. For an elaborated discussion and for technical details, we refer to Roeder and Loeffler (2002), Roeder (2003), and Roeder et al. (2006).

Applying this model to a number of different experimental scenarios, among them *in vivo* reconstitution (Roeder and Loeffler, 2002; Roeder et al., 2005), cell kinetics assays (Roeder and Loeffler, 2002), individual clone tracking (Roeder and Loeffler, 2002; Roeder et al., 2007), paired daughter cell assays (Roeder and Lorenz, 2006), and directed lineage specification *in vitro* (Glauche et al., 2007), we demonstrated that the proposed concept of hematopoietic stem cell organization consistently explains a broad variety of experimentally described phenomena.

Beyond these results, the model is also able to adequately describe clonal dynamics in the clinical context of hematopoietic disorders. Particularly, the model has been applied to chronic myeloid leukemia (CML), a clonal hematopoietic disorder induced by a chromosomal translocation generating the Philadelphia chromosome (Ph) and the oncogenic *BCR-ABL1* fusion gene. The translated BCR-ABL1 protein is responsible for an expansion of the malignant clone, resulting in the displacement of normal hematopoiesis (Mauro and Druker, 2001). Simulating leukemia expansion as well as treatment response, we were able to demonstrate the qualitative and quantitative adequacy of our model (Roeder et al., 2006; Horn et al., 2008). In particular, we could provide a consistent description of the *BCR-ABL1* transcript dynamics (as a measure of tumor size) in CML patients undergoing treatment with the tyrosine kinase inhibitor imatinib mesylate (IM), which is the current front-line therapy for *de novo* CML.

However, the proposed agent-based model (ABM) has the disadvantage that the computation time scales linearly with the maximum number of stem cells in the considered

system. This becomes specifically relevant if simulating realistic human systems with about 10^6 hematopoietic stem cells. Particularly, an adequate description of residual disease levels under (long-term) therapy with measurable proportions of less than one residual leukemia cell in 10^5 normal cells renders downscaling of the model system problematic. Therefore, we here suggest another mathematical representation of the proposed concept.Because the consideration of an "age"-structured rather than a homogeneous population of stem cells is a central point of our stem cell concept, we apply a partial differential equation (PDE) approach, which is considered as a standard method to describe the dynamics of structured populations (Metz and Diekmann, 1986). Using a system of PDEs, we are able to describe the average dynamics of the system independently of its size, i.e., the system can be simulated in constant time with regard to cell numbers. Although assuming a simplified model structure to facilitate an easier numerical processing, we show that such an approach is capable of reproducing the results obtained by the more complex ABM and that it provides a computationally efficient alternative.

The paper is structured as follows: First, we describe the general layout of the model. This is done for the situation of normal hematopoiesis. Thereafter, we will introduce model extensions that allow for the consideration of malignant cells (i.e., CML genesis) and, in a further step, for IM-affected malignant cells (i.e., IM treatment). This methodological part is completed by a description of the applied numerical procedures. What follows is the presentation of numerical simulations for the above mentioned scenarios (normal hematopoiesis, CML genesis, IM treatment) in comparison to the agent-based approach, and finally, a discussion of the results.

2. Model description

As already described above, HSCs are considered to reside in the two signaling contexts A and Ω. Furthermore, it is assumed that HSCs are heterogeneous with respect to their affinity for residing within these two contexts. This heterogeneity is described by the model variable a that characterizes the affinity of individual HSCs to reside within context A. More precisely, cells with a large value of a exhibit a high propensity to stay within A if they are in A or to change to A if they are in Ω. In contrast, cells with small a preferentially tend to avoid residence in A. Cells with $a < a_{\min}$ have completely lost their potential to reside in A and are, therefore, not regarded as stem cells anymore. See Fig. 1 for a graphical illustration.

To describe the dynamic changes of the two a-structured cell populations, we introduce

$$n_A(a,t) \quad \text{and} \quad n_\Omega(a,t), \tag{1}$$

denoting the cell densities at affinity a and time t within A and Ω, respectively. Stem cell numbers are obtained by integrating these functions with respect to affinity a. Because a is considered within the interval $[a_{\min}, a_{\max}]$ only, the integration can be restricted to this region, i.e.,

$$N_A(t) = N_A\big([a_{\min}, a_{\max}], t\big) = \int_{a_{\min}}^{a_{\max}} n_A(a,t)\,da, \tag{2}$$

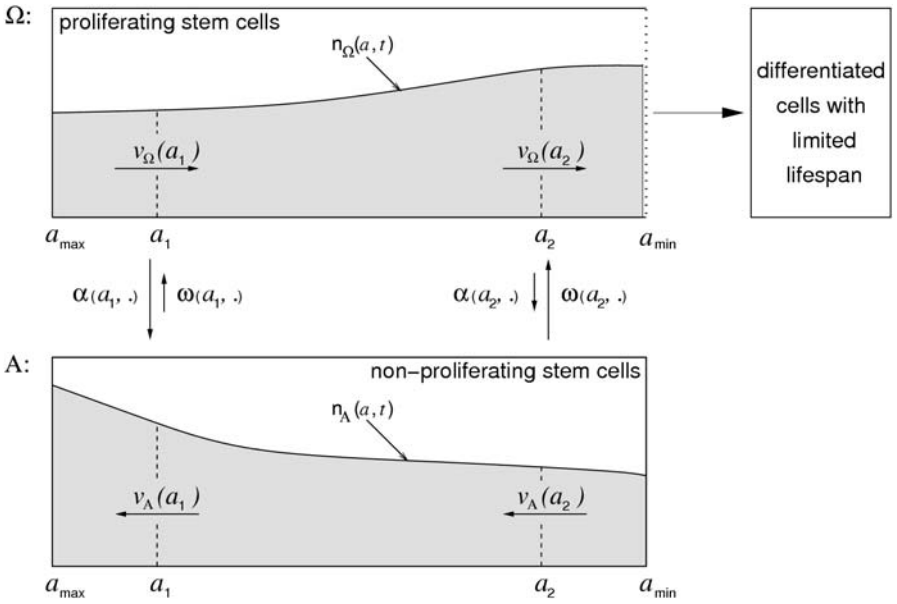

Fig. 1 Schematic representation of the mathematical model. Stem cells reside in two different signaling contexts, denoted as A and Ω, with proliferating cells located in Ω and quiescent cells located in A. The cell-intrinsic variable $a \in [a_{\min}, a_{\max}]$ denotes the propensity of a cell to reside in A. If a cell is located in A, its value of a is gradually increased over time up to a maximum value $a_{\max}$. The increase is dependent on a and described by velocity $v_A(a)$. In contrast, cells residing in Ω gradually decrease a, characterized by $v_\Omega(a)$. Any cell with $a < a_{\min}$ is no longer considered as a stem but as a differentiated cell with a limited lifespan. Transition rates between A and Ω are dependent on the position in the a-space as depicted by the differently sized arrows. For instance, cells in Ω with $a = a_1$ change to A at a higher rate than cells with $a = a_2$. Cell density functions of A and Ω are denoted as $n_A(a,t)$ and $n_\Omega(a,t)$, respectively. A detailed mathematical description of the model can be found in Section 2.

$$N_\Omega(t) = N_\Omega\big([a_{\min}, a_{\max}], t\big) = \int_{a_{\min}}^{a_{\max}} n_\Omega(a,t)\,da, \tag{3}$$

$$N(t) = N_A(t) + N_\Omega(t), \tag{4}$$

with N_A and N_Ω describing the number of stem cells in signaling context A and Ω, respectively, and N denoting the total number of HSCs in the system.

2.1. Normal hematopoiesis

For the derivation of the model equations, let us firstly consider the situation of normal hematopoiesis. Here, we assume only one cell type and no loss of stem cells despite the normal differentiation process (i.e., the decrease of a below $a_{\min}$ in Ω). Furthermore, let us start with considering the situation of no transition of cells between signaling contexts A and Ω.

Particularly for A, this means that there is no gain and no loss of cells. Hence, the cell number in a certain affinity interval $[a_1, a_2]$ at a given time point t_2 is fully determined by the cell number in the same affinity interval at a previous time point t_1 and the cell in-

and outfluxes during the considered time interval. The cell flux at point (a,t) is defined as $F(a,t) = n(a,t) \cdot v(a)$, e.g., in A it is characterized by velocity $v_A(a)$, see (11). Using this, we obtain

$$\int_{a_1}^{a_2} n_A(a,t_2)\,da = \int_{a_1}^{a_2} n_A(a,t_1)\,da + \int_{t_1}^{t_2} n_A(a_1,t)\cdot v_A(a_1)\,dt - \int_{t_1}^{t_2} n_A(a_2,t)\cdot v_A(a_2)\,dt. \tag{5}$$

Let us assume that $n_A(a,t)$ and $v_A(a)$ are differentiable functions. Then using

$$n_A(a,t_2) - n_A(a,t_1) = \int_{t_1}^{t_2} \frac{\partial}{\partial t} n_A(a,t)\,dt \tag{6}$$

and

$$n_A(a_2,t)\cdot v_A(a_2) - n_A(a_1,t)\cdot v_A(a_1) = \int_{a_1}^{a_2} \frac{\partial}{\partial a}\big(n_A(a,t)\cdot v_A(a)\big)\,da \tag{7}$$

in (5) gives

$$\int_{t_1}^{t_2}\int_{a_1}^{a_2} \left\{ \frac{\partial}{\partial t} n_A(a,t) + \frac{\partial}{\partial a}\big(n_A(a,t)\cdot v_A(a)\big)\right\} da\,dt = 0. \tag{8}$$

Because Eq. (8) holds for arbitrary affinity intervals $[a_1,a_2]$ and over any time interval $[t_1,t_2]$, one obtains the differential form of the conservation law for the number of cells in A

$$\frac{\partial}{\partial t} n_A(a,t) + \frac{\partial}{\partial a}\big(n_A(a,t)\cdot v_A(a)\big) = 0, \tag{9}$$

which can be rewritten as

$$\boxed{\frac{\partial}{\partial t} n_A(a,t) + v_A(a)\cdot \frac{\partial}{\partial a} n_A(a,t) = -\frac{d}{da} v_A(a)\cdot n_A(a,t).} \tag{10}$$

Herein, $v_A(a)$ denotes the velocity of increasing a, which is given by

$$v_A(a) = \begin{cases} \ln(r)\cdot a & \text{for } a < a_{\max}, \\ 0 & \text{for } a \geq a_{\max} \end{cases} \tag{11}$$

with regeneration coefficient $r \geq 1$.

To account for the assumption that there is no influx into A from cells with $a < a_{\min}$ (cf. Fig. 1), the following boundary condition is formulated:

$$n_A(a,t) = 0 \quad \text{for } a < a_{\min}. \tag{12}$$

The derivation of the differential equation governing the dynamics in Ω can be done analogously bearing in mind that in this context the velocity of changing a is negative

(a decreases with time) and that there is a source of cell production due to cell cycle activity. To avoid a further level of model complexity, the substructure of the cell cycle, which is explicitly considered in the ABM, is neglected in the PDE model. We model cell proliferation by an average cell division rate τ, which depends on the reciprocal of the average cell cycle duration τ_c, more precisely

$$\tau = \frac{\ln(2)}{\tau_c}. \tag{13}$$

The PDE describing the cell number dynamics within Ω can now be given as

$$\boxed{\frac{\partial}{\partial t} n_\Omega(a,t) + v_\Omega(a) \cdot \frac{\partial}{\partial a} n_\Omega(a,t) = \left(\tau - \frac{d}{da} v_\Omega(a)\right) \cdot n_\Omega(a,t).} \tag{14}$$

The velocity of losing a is defined by

$$v_\Omega(a) = -\ln(d) \cdot a \tag{15}$$

with differentiation coefficient $d \geq 1$.

To describe the model assumption of a maximum affinity $a_{\max}$, with no influx into Ω from cells with $a > a_{\max}$, the following boundary condition is formulated:

$$n_\Omega(a,t) = 0 \quad \text{for } a > a_{\max}. \tag{16}$$

In the following, the model equations are extended to comprise cell transitions from A to Ω and vice versa. As assumed in our general concept of stem cell organization and implemented in the agent-based system, each HSC has a certain probability per time step to change its context, with α denoting the probability for a change from Ω to A and ω for a change from A to Ω, respectively. These transition probabilities are dependent on the actual affinity a of the cell and on the number of cells in the target signaling context. If a cell does not change its context within a certain time step (with probabilities per time step $1-\alpha$ and $1-\omega$, respectively), it develops according to the particular rules of the corresponding context: change its affinity a (i.e., decrease in Ω / increase in A), and if in Ω, amplify due to cell division.

Additionally, it had been assumed in the agent-based system that transitions from Ω to A can only be realized during G_1-phase of the cell cycle (i.e., before starting the process of DNA synthesis in the so-called S-phase), and that transitions from A to Ω (which represent the reactivation of cells from the quiescent G_0-phase into active cell cycle) always result in an immediate initiation of S-phase. As we are aiming at a simple representation, the detailed cell cycle structure (i.e., the position of cells within the cell cycle) is neglected in the PDE model. For that reason, the cell cycle dependent context transition from Ω to A is modeled as a continuous process throughout the cell cycle. Technically, this is realized by weighting the transition function α by a factor κ, which represents the average proportion of the G_1-phase in relation to the total cell cycle duration.

With these assumptions, the transition rates from Ω to A and vice versa are defined as

$$\alpha = \alpha(a, N_A) = \kappa \cdot \frac{a}{a_{\max}} \cdot f_\alpha(N_A) \tag{17}$$

and

$$\omega = \omega(a, N_\Omega) = \frac{a_{\min}}{a} \cdot f_\omega(N_\Omega). \tag{18}$$

Following the formulation in the agent-based approach, the weight functions f_α and f_ω are modeled by a general class of sigmoid functions of the form

$$f(N) = \frac{1}{\nu_1 + \nu_2 \cdot \exp\left(\nu_3 \cdot \frac{N}{\tilde{N}}\right)} + \nu_4. \tag{19}$$

The parameters ν_1, ν_2, ν_3, and ν_4 determine the shape of f, and $\tilde{N}$ is a scaling factor for N. It is possible to uniquely determine ν_1, ν_2, ν_3, and ν_4 by fixing the more intuitive values $f(0)$, $f(\tilde{N}/2)$, $f(\tilde{N})$, and $f(\infty) := \lim_{N\to\infty} f(N)$:

$$\nu_1 = \left(h_1 h_3 - h_2^2\right)\big/(h_1 + h_3 - 2h_2), \qquad \nu_2 = h_1 - \nu_1,$$
$$\nu_3 = \ln\left((h_3 - \nu_1)/\nu_2\right), \qquad \nu_4 = f(\infty)$$

with the dummy variables

$$h_1 = 1/\left[f(0) - f(\infty)\right], \qquad h_2 = 1/\left[f(\tilde{N}/2) - f(\infty)\right],$$
$$h_3 = 1/\left[f(\tilde{N}) - f(\infty)\right].$$

Suppl. Fig. B.1 provides a graphical illustration of the transition rates and their functional relationship on the HSC numbers N_A and N_Ω, and on the context affinity a.

Now, the complete system of PDEs describing the HSC dynamics in the situation of normal hematopoiesis can be written as follows (function arguments are omitted for reasons of brevity):

$$\boxed{\begin{aligned} \frac{\partial}{\partial t} n_A + v_A \cdot \frac{\partial}{\partial a} n_A &= \left(-\frac{d}{da} v_A - \omega\right) \cdot n_A + \alpha \cdot n_\Omega, \\ \frac{\partial}{\partial t} n_\Omega + v_\Omega \cdot \frac{\partial}{\partial a} n_\Omega &= \left(-\frac{d}{da} v_\Omega + \tau - \alpha\right) \cdot n_\Omega + \omega \cdot n_A. \end{aligned}} \tag{20}$$

2.2. *Leukemia genesis*

For leukemia genesis, we now consider the situation of two different types of stem cells: normal and leukemia cells. We, therefore, introduce additional equations for leukemia stem cells. The structure of these equations is identical to those formulated in the previous section. However, as model parameters are expected to differ between normal and leukemia cells, we additionally introduce superscripts ("1" for normal, "2" for leukemia cells) to refer to the different cell types:

$$\boxed{\begin{aligned} \frac{\partial}{\partial t} n_A^{(1,2)} + v_A^{(1,2)} \cdot \frac{\partial}{\partial a} n_A^{(1,2)} &= \left(-\frac{d}{da} v_A^{(1,2)} - \omega^{(1,2)}\right) \cdot n_A^{(1,2)} + \alpha^{(1,2)} \cdot n_\Omega^{(1,2)}, \\ \frac{\partial}{\partial t} n_\Omega^{(1,2)} + v_\Omega^{(1,2)} \cdot \frac{\partial}{\partial a} n_\Omega^{(1,2)} &= \left(-\frac{d}{da} v_\Omega^{(1,2)} + \tau^{(1,2)} - \alpha^{(1,2)}\right) \cdot n_\Omega^{(1,2)} + \omega^{(1,2)} \cdot n_A^{(1,2)}. \end{aligned}} \tag{21}$$

The definitions of $v_A(a)$ and $v_\Omega(a)$ can be intuitively extended to the situation of two cell types, i.e., $v_A^{(j)}(a)$ and $v_\Omega^{(j)}(a)$ for $j \in \{1,2\}$, bearing in mind that the velocities are now calculated using $r^{(j)}$ and $d^{(j)}$, respectively. Similarly, $\tau^{(j)}$ is defined by a cell type specific average cycle time $\tau_c^{(j)}$ and the proportion of G_1-phase of cell type j is denoted by $\kappa^{(j)}$. Transition rates $\alpha^{(j)}$ and $\omega^{(j)}$ include cell type specific weight functions $f_\alpha^{(j)}$ and $f_\omega^{(j)}$, respectively.

The total number of cells in the system N is given by $N(t) = N_A(t) + N_\Omega(t)$. Please note the generalized definitions of cell numbers N_A and N_Ω:

$$N_A(t) = \sum_{j=1,2} N_A^{(j)}(t) \quad \text{and} \quad N_\Omega(t) = \sum_{j=1,2} N_\Omega^{(j)}(t), \tag{22}$$

with

$$N_A^{(j)}(t) = \int_{a_{\min}}^{a_{\max}} n_A^{(j)}(a,t)\,da \quad \text{and} \quad N_\Omega^{(j)}(t) = \int_{a_{\min}}^{a_{\max}} n_\Omega^{(j)}(a,t)\,da. \tag{23}$$

2.3. Leukemia treatment

Imatinib mesylate (IM) is described as a compound that specifically targets leukemic (e.g., *BCR-ABL1* positive) cells (Buchdunger et al., 1996; Savage and Antman, 2002). It has two major effects, proliferation inhibition (Druker et al., 1996) and cell death induction (Vigneri and Wang, 2001). Furthermore, it has been reported that IM only targets proliferating cells (Jørgensen et al., 2006; Holtz et al., 2007).

Based on these observations, we model proliferation inhibition by an altered transition weight function f_ω for leukemic cells, if they are affected by IM. Particularly, we assume that only proliferating leukemic cells, i.e., those in Ω, are affected by IM with a constant rate r_{inh}. In order to distinguish IM-affected and unaffected leukemic cells, a third cell type (superscript "3") is introduced. The second treatment effect, namely the induced cell death, is modeled by a constant degradation rate r_{deg}, which affects all leukemic cells in Ω.

Based on these assumptions, the following set of equations is obtained:

$$\begin{aligned}
&\frac{\partial}{\partial t} n_A^{(1,2,3)} + v_A^{(1,2,3)} \frac{\partial}{\partial a} n_A^{(1,2,3)} = \left(-\frac{d}{da} v_A^{(1,2,3)} - \omega^{(1,2,3)} \right) n_A^{(1,2,3)} + \alpha^{(1,2,3)} n_\Omega^{(1,2,3)},\\
&\frac{\partial}{\partial t} n_\Omega^{(1)} + v_\Omega^{(1)} \frac{\partial}{\partial a} n_\Omega^{(1)} = \left(-\frac{d}{da} v_\Omega^{(1)} + \tau^{(1)} - \alpha^{(1)} \right) n_\Omega^{(1)} + \omega^{(1)} n_A^{(1)},\\
&\frac{\partial}{\partial t} n_\Omega^{(2)} + v_\Omega^{(2)} \frac{\partial}{\partial a} n_\Omega^{(2)} = \left(-\frac{d}{da} v_\Omega^{(2)} + \tau^{(2)} - \alpha^{(2)} - r_{\text{inh}} - r_{\text{deg}} \right) n_\Omega^{(2)} + \omega^{(2)} n_A^{(2)},\\
&\frac{\partial}{\partial t} n_\Omega^{(3)} + v_\Omega^{(3)} \frac{\partial}{\partial a} n_\Omega^{(3)} = \left(-\frac{d}{da} v_\Omega^{(3)} + \tau^{(3)} - \alpha^{(3)} - r_{\text{deg}} \right) n_\Omega^{(3)} + \omega^{(3)} n_A^{(3)} + r_{\text{inh}} \cdot n_\Omega^{(2)}.
\end{aligned} \tag{24}$$

3. Numerics

3.1. PDE solution

Without loss of generality, the numerical procedure is described for the case of one cell type only. This procedure, however, can be generalized in a straight forward manner to two or more cell types, as required for the situation of CML genesis or treatment.

In case of no cellular traffic between contexts A and Ω (i.e., $f_\alpha \equiv 0$, $f_\omega \equiv 0$), the two PDEs specified in (20) can be analytically solved independently of each other using the *method of characteristics* (LeVeque, 1990). The initial value problem (IVP) for context A is given as

$$\boxed{\begin{aligned} \frac{\partial}{\partial t} n_A(a,t) + v_A(a) \cdot \frac{\partial}{\partial a} n_A(a,t) &= -\frac{d}{da} v_A(a) \cdot n_A(a,t), \\ n_A(a,0) &= \tilde{n}_A(a), \end{aligned}} \tag{25}$$

with $\tilde{n}_A(a)$ describing the initial distribution of cells with respect to affinity a at time $t = 0$. Because only cells with $a \in [a_{\min}, a_{\max}]$ are considered, we set $\tilde{n}_A(a) = 0 \ \forall a \notin [a_{\min}, a_{\max}]$.

The characteristic equations of problem (25), in their parametric form, are given by

$$\frac{dt}{ds} = 1, \qquad \frac{da}{ds} = v_A(a), \qquad \frac{dn_A}{ds} = -\frac{d}{da} v_A(a) \cdot n_A(a,t). \tag{26}$$

Using definition (11), the characteristics within the interval $[a_{\min}, a_{\max}]$ can be described as

$$a(t) = \begin{cases} a(0) \cdot r^t = a_0 \cdot r^t & \text{for } a \in [a_{\min}, a_{\max}), \\ a_{\max} & \text{for } a = a_{\max}. \end{cases} \tag{27}$$

In order to solve the IVP, $n_A(a,t)$ is differentiated along these characteristics. For the half-closed interval $[a_{\min}, a_{\max})$, one obtains from Eqs. (26)

$$\frac{d}{dt} n_A\big(a(t), t\big) = -\frac{d}{da} v_A(a) \cdot n_A\big(a(t), t\big), \tag{28}$$

which can be solved for n_A with the result:

$$n_A(a,t) = \tilde{n}_A(a) \cdot r^{-t}. \tag{29}$$

From (27), one can explicitly calculate the initial value a_0 obtaining

$$n_A(a,t) = n_A\big(a \cdot r^{-t}, 0\big) \cdot r^{-t}. \tag{30}$$

For the initial condition specified in (25), the solution of the PDE is

$$n_A(a,t) = \tilde{n}_A\big(a \cdot r^{-t}\big) \cdot r^{-t} \quad \text{for } a \in [a_{\min}, a_{\max}) \tag{31}$$

and the cell number in a given interval $[a_1, a_2]$ with $a_{\min} \le a_1 \le a_2 < a_{\max}$ can be calculated by

$$N_A\big([a_1, a_2], t\big) = \int_{a_1}^{a_2} n_A(a,t)\, da = \int_{a_1}^{a_2} \tilde{n}_A\big(a \cdot r^{-t}\big) \cdot r^{-t}\, da. \tag{32}$$

Substituting $a \cdot r^{-t} = s$ and subsequently renaming $s = a$, this can also be written as

$$N_A\big([a_1, a_2], t\big) = \int_{a_1 r^{-t}}^{a_2 r^{-t}} \tilde{n}_A(a)\, da. \tag{33}$$

So far, the point $a = a_{\max}$ has been excluded from the solution. To account for the particular situation that all cells reaching $a_{\max}$ cumulate at this point, the cell density at $a_{\max}$ is represented by a Dirac δ-function (Spanier and Oldham, 1987):

$$n_A(a_{\max}, t) = C \cdot \delta(a - a_{\max}) \quad \text{with } C = \int_{a_{\max} r^{-t}}^{a_{\max}} \tilde{n}_A(a)\, da. \tag{34}$$

Using (34), it is now possible to calculate the number of cells for intervals which include $a_{\max}$, and thus the cell numbers in A are generally obtained by

$$N_A\big([a_1, a_2], t\big) = \begin{cases} \int_{a_1 r^{-t}}^{a_2 r^{-t}} \tilde{n}_A(a)\, da & \text{for } a_1, a_2 < a_{\max}, \\ \int_{a_1 r^{-t}}^{a_{\max}} \tilde{n}_A(a)\, da & \text{for } a_1 \le a_{\max},\ a_2 = a_{\max}. \end{cases} \tag{35}$$

For context Ω, the following IVP has to be considered:

$$\boxed{\begin{gathered} \frac{\partial}{\partial t} n_\Omega(a,t) + v_\Omega(a) \cdot \frac{\partial}{\partial a} n_\Omega(a,t) = \left(\tau - \frac{d}{da} v_\Omega(a)\right) \cdot n_\Omega(a,t), \\ n_\Omega(a,0) = \tilde{n}_\Omega(a). \end{gathered}} \tag{36}$$

Similar to $\tilde{n}_A(a)$ in A, $\tilde{n}_\Omega(a)$ describes the initial a-distribution of cells in Ω with $\tilde{n}_\Omega(a) = 0$ for all $a \notin [a_{\min}, a_{\max}]$. In analogy to context A, the *method of characteristics* is applied to solve the IVP. Along the characteristic curves, which are given by

$$a(t) = a_0 \cdot d^{-t}, \tag{37}$$

the PDE reduces to an ordinary differential equation (ODE) with the solution

$$n_\Omega(a,t) = \tilde{n}_\Omega\big(a \cdot d^t\big) \cdot e^{(\ln(d)+\tau)\cdot t}, \tag{38}$$

and using (13) the cell numbers in the interval $[a_1, a_2]$ can be calculated by

$$N_\Omega\big([a_1, a_2], t\big) = 2^{t/\tau_c} \cdot \int_{a_1 d^t}^{a_2 d^t} \tilde{n}_\Omega(a)\, da. \tag{39}$$

Let us now turn to the more relevant situation of non-zero transitions between A and Ω. To the best of our knowledge, it is not feasible to analytically solve the system of two coupled nonlinear PDEs (20). Furthermore, due to the different "velocities" of the transport

processes (modeled by differentiation rate d in Ω and regeneration rate r in A), standard numerical schemes cannot be applied. Hence, the following procedure to approximate the solution iteratively for small time steps Δt is proposed:

We assume the functions $f_\alpha(N_A)$ and $f_\omega(N_\Omega)$ as well as $\kappa(N)$ and $\tau_c(N)$ to be constant during the time intervals Δt, i.e., $\hat{f}_\alpha \equiv f_\alpha(N_A(t))$, $\hat{f}_\omega \equiv f_\omega(N_\Omega(t))$, $\hat{\kappa} \equiv \kappa(N(t))$ and $\hat{\tau}_c \equiv \tau_c(N(t))$ for all $t \in [t, t+\Delta t)$. Introducing this assumption into reduced versions of the model equations, which neglect the influx terms from the opposite context, one obtains the following two uncoupled PDEs for n_A and n_Ω:

$$\frac{\partial}{\partial t} n_A(a,t) + v_A(a) \cdot \frac{\partial}{\partial a} n_A(a,t) = \left(-\frac{d}{da} v_A(a) - \frac{a_{\min}}{a} \cdot \hat{f}_\omega \right) \cdot n_A(a,t), \tag{40}$$

$$\begin{aligned} &\frac{\partial}{\partial t} n_\Omega(a,t) + v_\Omega(a) \cdot \frac{\partial}{\partial a} n_\Omega(a,t) \\ &\quad = \left(-\frac{d}{da} v_\Omega(a) + \frac{\ln(2)}{\hat{\tau}_c} - \hat{\kappa} \cdot \frac{a}{a_{\max}} \cdot \hat{f}_\alpha \right) \cdot n_\Omega(a,t). \end{aligned} \tag{41}$$

These equations can be solved analytically, again using the *method of characteristics*. To determine the cell density within A one has to solve the following ODE:

$$\begin{aligned} \frac{d}{dt} n_A\big(a(t),t\big) &= \left(-\ln(r) - \frac{a_{\min}}{a(t)} \cdot \hat{f}_\omega \right) \cdot n_A(t) \\ &= \left(-\ln(r) - \frac{a_{\min}}{a_0 \cdot r^t} \cdot \hat{f}_\omega \right) \cdot n_A(t), \end{aligned} \tag{42}$$

leading to

$$n_A(t) = C_0 \cdot e^{\frac{a_{\min} \cdot \hat{f}_\omega \cdot r^{-t}}{a_0 \cdot \ln(r)} - \ln(r) \cdot t}. \tag{43}$$

Using furthermore

$$n_A(t=0) = C_0 \cdot e^{\frac{a_{\min} \cdot \hat{f}_\omega}{a_0 \cdot \ln(r)}} \tag{44}$$

one finally obtains

$$n_A\big(a(t),t\big) = n_A(a_0,0) \cdot e^{\frac{a_{\min} \cdot \hat{f}_\omega}{a_0 \cdot \ln(r)} (r^{-t} - 1)} \cdot r^{-t}. \tag{45}$$

Similarly, one can derive the cell density within Ω, neglecting the influx from the opposite signaling context A. Here, the corresponding ODE is given by

$$\begin{aligned} \frac{d}{dt} n_\Omega\big(a(t),t\big) &= \left(\ln(d) + \frac{\ln(2)}{\hat{\tau}_c} - \hat{\kappa} \cdot \frac{a(t)}{a_{\max}} \cdot \hat{f}_\alpha \right) \cdot n_\Omega(t) \\ &= \left(\ln(d) + \frac{\ln(2)}{\hat{\tau}_c} - \hat{\kappa} \cdot \frac{a_0 \cdot d^{-t}}{a_{\max}} \cdot \hat{f}_\alpha \right) \cdot n_\Omega(t), \end{aligned} \tag{46}$$

which has the solution

$$n_\Omega\big(a(t),t\big) = n_\Omega(a_0,0)\cdot e^{\frac{\hat\kappa\cdot a_0\cdot \hat f_\alpha}{a_{\max}\cdot\ln(d)}(d^{-t}-1)}\cdot d^t\cdot 2^{t/\hat\tau_c}. \tag{47}$$

To complete the solutions (45) and (47) by adding the influx terms, we use the fact that the influx into one context equals the outflux of the other. Furthermore, the outfluxes can be determined by the density differences obtained from the solutions of the uncoupled system without any transition (25), (36) and with outfluxes only (40), (41). Using this, we approximate the flux terms for each time step Δt by the proportions

$$\frac{1}{\big(1-e^{\frac{a_{\min}\cdot\hat f_\omega}{a(t)\cdot\ln(r)}\cdot(1-r^{\Delta t})}\big)}\cdot n_A\big(a(t),t\big) \tag{48}$$

and

$$\frac{1}{\big(1-e^{\frac{\hat\kappa\cdot a(t)\cdot\hat f_\alpha}{a_{\max}\cdot\ln(d)}\cdot(1-d^{\Delta t})}\big)}\cdot n_\Omega\big(a(t),t\big), \tag{49}$$

and we obtain the following rules for an iterative calculation of densities n_A and n_Ω:

$$\begin{aligned}
n_A(a,t+\Delta t) &= n_A\big(a\cdot r^{-\Delta t},t\big)\cdot e^{\frac{a_{\min}\cdot\hat f_\omega}{a\cdot\ln(r)}\cdot(1-r^{\Delta t})}\cdot r^{-\Delta t}+\cdots\\
&\quad+\big(1-e^{\frac{\hat\kappa\cdot a\cdot\hat f_\alpha}{a_{\max}\cdot\ln(d)}\cdot(1-d^{\Delta t})}\big)\cdot n_\Omega(a,t),\\
n_\Omega(a,t+\Delta t) &= n_\Omega\big(a\cdot d^{\Delta t},t\big)\cdot e^{\frac{\hat\kappa\cdot a\cdot\hat f_\alpha}{a_{\max}\cdot\ln(d)}\cdot(1-d^{\Delta t})}\cdot d^{\Delta t}\cdot 2^{\Delta t/\hat\tau_c}+\cdots\\
&\quad+\big(1-e^{\frac{a_{\min}\cdot\hat f_\omega}{a\cdot\ln(r)}\cdot(1-r^{\Delta t})}\big)\cdot n_A(a,t).
\end{aligned} \tag{50}$$

The initial densities are given as $n_A(a,0)=\tilde n_A(a)$ and $n_\Omega(a,0)=\tilde n_\Omega(a)$.

As mentioned above, the cells in A accumulate at the point $a=a_{\max}$ due to the assumption $v_A(a_{\max})=0$. The arising density discontinuity may cause stiffness problems when using numerical integration methods. To attenuate this problem, we redistribute the cells which accumulate at $a_{\max}$ during Δt, over the interval $[a_{\max}\cdot r^{-\Delta t}, a_{\max}]$. More precisely, we consider $\hat N_\Omega \equiv N_\Omega(t)$ within the small time interval Δt. Following (18), we furthermore consider a constant transition rate $\hat\omega=\omega(a_{\max},\hat N_\Omega)$ within Δt. Hence, the number of cells to be redistributed, i.e., the number of cells piling up at $a_{\max}$ less those cells changing to Ω during Δt, is given as

$$\hat N_A^{\mathrm{re}} = (1-\hat\omega)\cdot\int_{a_{\max}\cdot r^{-\Delta t}}^{a_{\max}} n_A(a,t)\,da. \tag{51}$$

After calculating $n_A(a,t+\Delta t)$ and $n_\Omega(a,t+\Delta t)$ according to the iterative procedure given in (50), we redistribute $\hat N_A^{\mathrm{re}}$ over the interval $[a_{\max}\cdot r^{-\Delta t}, a_{\max}]$ using a triangular

density function. That means, we apply a linear function $\phi(a)$ with its maximum value in the interval at $a = a_{\max}$, its root at $a = a_{\max} \cdot r^{-\Delta t}$ and the additional property

$$\int_{a_{\max} \cdot r^{-\Delta t}}^{a_{\max}} \phi(a)\, da = \hat{N}_A^{\mathrm{re}}. \tag{52}$$

$\phi(a)$ can be uniquely determined and written as

$$\phi(a) = \frac{2\hat{N}_A^{\mathrm{re}} \cdot r^{\Delta t}(a \cdot r^{\Delta t} - a_{\max})}{[a_{\max}(r^{\Delta t} - 1)]^2}. \tag{53}$$

The redistribution is realized by a redefinition of the density n_A at time $t + \Delta t$:

$$n_A(a, t + \Delta t) := \begin{cases} n_A(a, t + \Delta t) + \phi(a) & \text{for } a \in [a_{\max} \cdot r^{-\Delta t}, a_{\max}), \\ \phi(a) & \text{for } a = a_{\max}, \\ n_A(a, t + \Delta t) & \text{else.} \end{cases} \tag{54}$$

For numerical purposes, we discretize the a-space $[a_{\min}, a_{\max}]$ using an equidistant grid with

$$\Delta a = \frac{a_{\max} - a_{\min}}{n - 1}, \quad n > 1. \tag{55}$$

The grid points are denoted by $a_{\min} + j\Delta a$, $j \in \{0, \ldots, n - 1\}$. Values of a are always rounded to the closest grid point. To numerically integrate over any interval $[a_1, a_2]$, $a_i = a_{\min} + j\Delta a$, we use Simpson's rule (Atkinson, 1989) for $m \geq 1$ subintervals $[a_1 + 2k\Delta a, a_1 + 2(k + 1)\Delta a]$ with $k \in \{0, \ldots, m - 1\}$ and $a_1 + 2m\Delta a = a_2$. The odd multiples of Δa, denoted by $a_1 + (2k + 1)\Delta a$, are used as subinterval midpoints, respectively, as required in the standard procedure. It follows that for m subintervals, the number of corresponding grid points is $2m + 1$, which has the consequence that each integral has to be calculated using an uneven number of grid points. In our numerical calculations, we set $n = 7993$, resulting in grid width $\Delta a \approx 1.2487 \cdot 10^{-4}$. This particular number of grid points has proven to be a good trade-off between accuracy and calculation time. Furthermore, it guarantees that all applications of Simpson's rule in the algorithm fulfill the requirements regarding unevenness. Finally, applying this particular partitioning, there exists a grid point $a_{\min} + j\Delta a$, which almost exactly coincides with $a = a_{\max} \cdot r^{-\Delta t}$ if using the parameter values given in Table A.1 (see Appendix A). Due to the latter, an additional reduction of potential numerical problems can be achieved when performing the redistribution procedure described in (54).

Discretization of time in our implementation is $\Delta t = 1$ hour, which is the value used in the agent-based model. A higher time resolution has only minor influences on the results.

Parameters κ and τ_c were estimated from the ABM by computer simulation. To do so, we recorded the average cell cycle times τ_c (excluding G_0) and the corresponding G_1-phase proportions $\kappa = \tau_{G_1}/\tau_c$ for the growth scenario described in Section 4.1. Both parameters are now considered as functions of the total cell number N. This represents a simplifying assumption, i.e., τ_c and κ do not exclusively depend on N, but also on the distribution of cells with respect to affinity a. The dependencies are described by the following general class of sigmoid functions:

$$f(N) = \frac{\lambda_1}{1 + \lambda_2 \cdot \exp(-\lambda_3 \cdot N)} + \lambda_4. \tag{56}$$

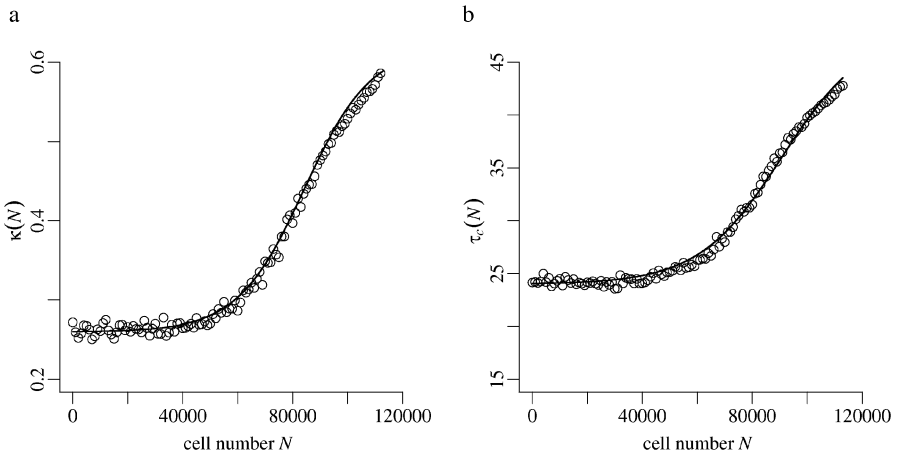

Fig. 2 Scatterplots depicting the functional correlation between G_1-phase proportion κ and total cell number N (panel a) as well as between cell cycle duration τ_c and N (panel b). Both scatterplots are derived from the agent-based model by computer simulation. The solid lines show fits of a general class of sigmoid functions (as defined in (56)) to the respective data.

Fitting these functions to the simulated data points leads to the following parameters: For $\kappa(N)$, we obtain $\lambda_1 = 0.36$, $\lambda_2 = 1000$, $\lambda_3 = 8.2 \cdot 10^{-5}$, and $\lambda_4 = 0.26$; for $\tau_c(N)$, we obtain $\lambda_1 = 24$, $\lambda_2 = 400$, $\lambda_3 = 6.6 \cdot 10^{-5}$, and $\lambda_4 = 24$. Figure 2 illustrates the functional relationships.

To be able to perform numerical simulations, the above described iterative procedure for calculating the cell numbers in A and Ω has been implemented in a C++ program.

3.2. Simulation

The exact parameter values used in our calculations can be found in Table A.1 in Appendix A. For comparison purposes, we use the same parameters as in the ABM, unless indicated otherwise.

To determine the size of the tumor burden in patients, *BCR-ABL1* transcript levels are determined. To obtain these values, transcripts of the *BCR-ABL1* oncogene are quantified using quantitative polymerase chain reaction (PCR) techniques. In order to compensate for variations in the amplification efficiency, the number of *BCR-ABL1* transcripts is normalized using the number of transcripts of a control gene, e.g., *ABL1* (Hochhaus et al., 2000). As a strong correlation of the proportion of *BCR-ABL1* positive cells and quantitative PCR measurements of *BCR-ABL1* transcript levels has been reported (Branford et al., 1999), we can use the proportion of leukemic cells in order to estimate *BCR-ABL1* transcript levels in the model simulations.

In the clinical situation, *BCR-ABL1* transcript levels are determined using peripheral blood cells. However, for the sake of simplicity, our mathematical model is restricted to the description of the dynamics of HSCs. As we assume that dynamic regulations on the stage of more differentiated cells equally affect normal and leukemic cells, they do not change their relative proportion, which justifies to neglect an explicit modeling of the more mature cell stages. Instead, we use those cells that are about to leave the stem cell

compartment, i.e., cells in Ω with $a \approx a_{\min}$, to determine *BCR-ABL1* levels in the model by calculating the proportion of leukemic cells L:

$$L(t) = \frac{\hat{N}_{\Omega}^{(2)}(t) + \hat{N}_{\Omega}^{(3)}(t)}{(\hat{N}_{\Omega}^{(2)}(t) + \hat{N}_{\Omega}^{(3)}(t)) + 2 \cdot \hat{N}_{\Omega}^{(1)}(t)} \cdot 100\%, \tag{57}$$

with

$$\hat{N}_{\Omega}^{(j)}(t) = \int_{a_{\min}}^{a_2} n_{\Omega}^{(j)}(a,t)\, da \tag{58}$$

denoting the numbers of normal cells ($j = 1$), IM-unaffected leukemic cells ($j = 2$), and IM-affected leukemic cells ($j = 3$) within the interval $[a_{\min}, a_2]$, respectively. Particularly, we herein consider $a_2 = 0.1019$, which represents approximately one tenth of the Ω context (cf. Fig. 1). This particular a_2-choice also coincides with grid point $a_{\min} + j\Delta a$ for $j = 800$, which guarantees an uneven number of grid points included in the interval as required by the above described implementation of Simpson's rule. It can be demonstrated (data not shown) that the cells within this interval adequately represent the composition of differentiating cells because the transition from and to A can be neglected for these cells.

4. Results

4.1. Normal hematopoiesis

To study the development from a few cells to steady-state hematopoiesis, we start with 10 uniformly distributed cells both in A and Ω, i.e., $\tilde{n}_A$ and $\tilde{n}_{\Omega}$ are chosen as constants over $[a_{\min}, a_{\max}]$. To check whether the averaged system behavior of the ABM can be reproduced by the PDE model, firstly, the parameter configuration which has shown to produce a stable system in the single cell-based approach is considered. More precisely, we use the parameter values given in Table A.1 and the empirically determined functional relationships $\tau_c(N)$ and $\kappa(N)$, which are depicted in Fig. 2 by the solid lines, to numerically solve Eqs. (20).

Using this parameter configuration, the growth phase is significantly delayed in the PDE model compared to the ABM. Moreover, the PDE model underestimates the cell numbers in the steady-state situation, especially for the Ω context, which points to an insufficiently low cell division rate τ (data not shown). This deficiency can be compensated by reducing the average cell cycle time $\tau_c(N)$ (Fig. 2b) by a constant shift. More precisely, we reduce λ_4 in Eq. (56) from 24 to 16. Using this modified function, which is depicted in Suppl. Fig. B.2, a perfect agreement between the PDE and the average ABM solution with respect to steady-state stem cell numbers is achieved (see Fig. 3).

However, there are still some quantitative differences in the growth phase of the system. Most strikingly, a transient oscillatory behavior for intermediate stem cell numbers can be observed in context Ω. This dynamical artefact can be explained by the particular choice of the nonlinear functions $\kappa(N)$ and $f_{\alpha}(N_A)$. Specifically, the product $\kappa \cdot f_{\alpha}$, which is used within (50) to calculate the loss or gain of cells in Ω, exhibits a changing monotonicity at about $t = 1$ year (see Suppl. Fig. B.3), resulting in the observed transient decrease of cell numbers followed by a subsequent increase. Thus, the quantitative discrepancy can most likely be attributed to the fact that the empirically determined

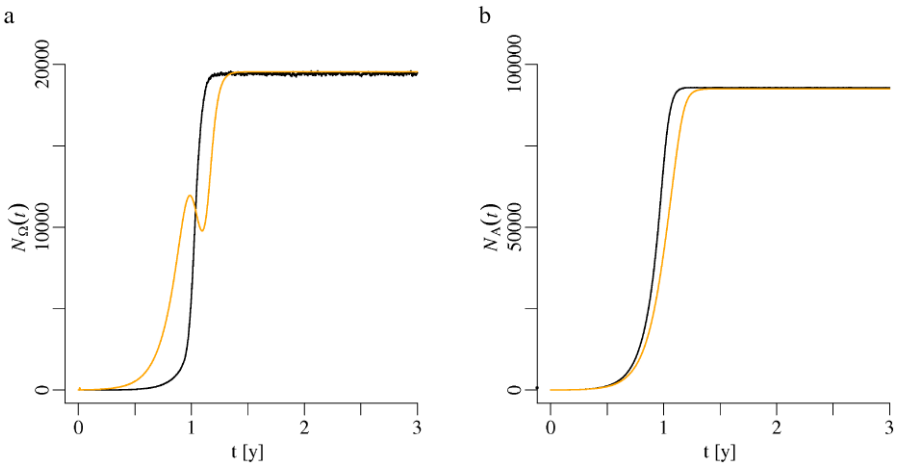

Fig. 3 Simulation of steady-state hematopoiesis, starting from only a few stem cells, with respect to cell numbers in contexts Ω (panel a) and A (b). The black lines depict averages of 20 ABM simulation runs, whereas the orange lines show the corresponding numerical solutions of the PDE model. (Color figure online.)

functional relationship $\kappa(N)$ only incompletely reflects the dynamic regulation of the G_1-phase in the agent-based system. However, as this transient behavior is only observed for the situation of a regenerating system at a stage of rather low cell numbers, which is neither relevant for the situation of leukemia genesis nor treatment, we use this parameter configuration for all subsequent scenarios in this paper.

4.2. Leukemia genesis

In order to simulate CML genesis, we start from a normal steady-state hematopoiesis, i.e., the initial distributions of normal cells in A and Ω, denoted by $\tilde{n}_A^{(1)}(a)$ and $\tilde{n}_\Omega^{(1)}(a)$, equal the cell densities $n_A(a,t)$ and $n_\Omega(a,t)$ obtained at the steady-state in Section 4.1, respectively. We assume that CML is induced by a single-cell mutation, i.e., by the introduction of one malignant Ω stem cell. Without loss of generality we, therefore, set $\tilde{n}_\Omega^{(2)} \equiv 1/(a_{\max} - a_{\min})$ and $\tilde{n}_A^{(2)} \equiv 0$.

As described in Roeder et al. (2006), we assume leukemia cells to be characterized by defective mechanisms regarding quiescence and activation into active cell cycle. More precisely, weight function $f_\alpha^{(2)}$, which describes the transition of leukemia cells to the A context, is modified. For the exact parameter values we refer to Table A.1. See Suppl. Fig. B.4a for a graphical representation. Furthermore, weight function $f_\omega^{(2)}$, which describes the activation of quiescent leukemia cells into a proliferative state, is considered almost constant at a high level (Suppl. Fig. B.4b). As a result, the activation of leukemia cells is unregulated, i.e., independent of N_Ω.

Using the modified τ_c function (as described in Section 4.1) for both normal and leukemia cells in the PDE model, the time to a manifest leukemia is considerably longer than observed in the agent-based approach. Moreover, the cell numbers of leukemia cells are underestimated by the PDE model owing to an insufficient cell amplification rate (data not shown). This can be counteracted by modifying τ_c of leukemia cells. To achieve an in-

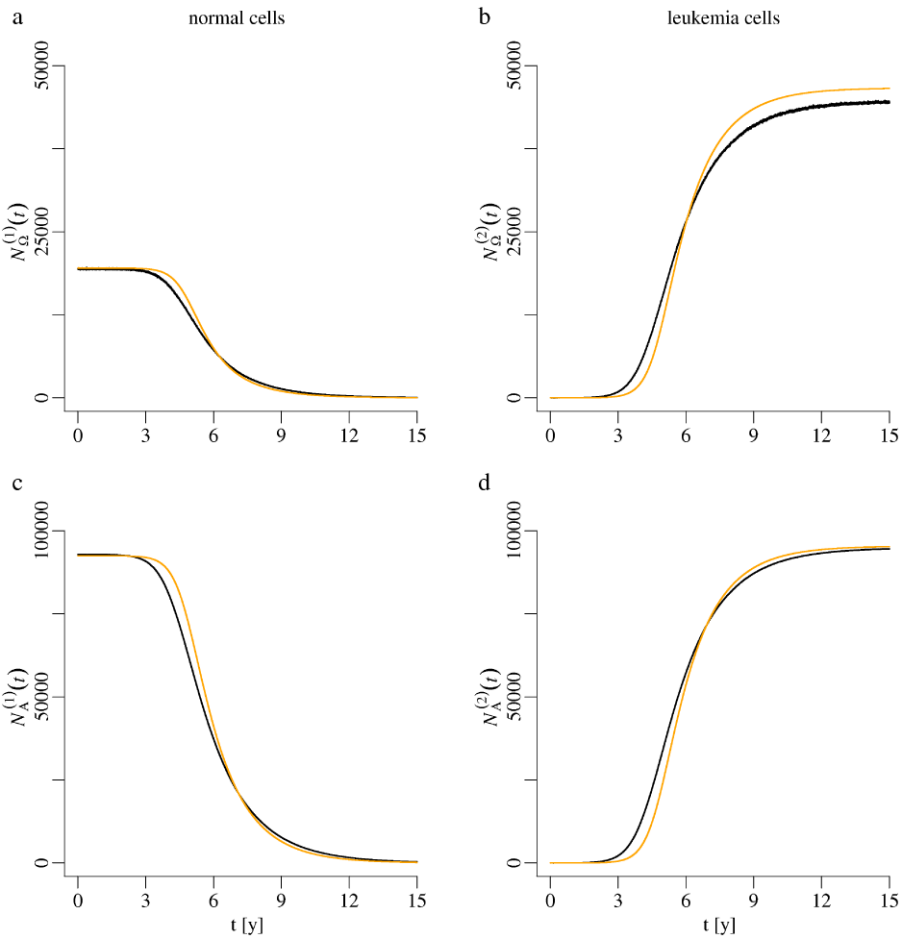

Fig. 4 Cell numbers of normal (cell type "1") and leukemia cells (type "2"), separated by signaling contexts Ω (above) and A (below), respectively, for the genesis of CML. The black curves represent averages of 20 ABM simulations, whereas the orange curves depict numerical solutions of the PDE model. (Color figure online.)

creased amplification of leukemic cells, we slightly adjusted the cell cycle function $\tau_c(N)$. Particularly, we set $\lambda_1 = 19$ in Eq. (56). The modified function is shown in Suppl. Fig. B.2.

As illustrated in Fig. 4, a good agreement of ABM and PDE model can be achieved using this modification. However, the PDE model seems to slightly overestimate the number of malignant Ω cells in the long run, probably owing to the simplified representation of the cell cycle.

4.3. Leukemia treatment

The simulation of IM treatment is initiated with cell densities $\tilde{n}_A^{(1,2)}(a) = n_A^{(1,2)}(a, \tilde{t})$ and $\tilde{n}_\Omega^{(1,2)}(a) = n_\Omega^{(1,2)}(a, \tilde{t})$, where $\tilde{t}$ denotes the time at which the hematopoietic system con-

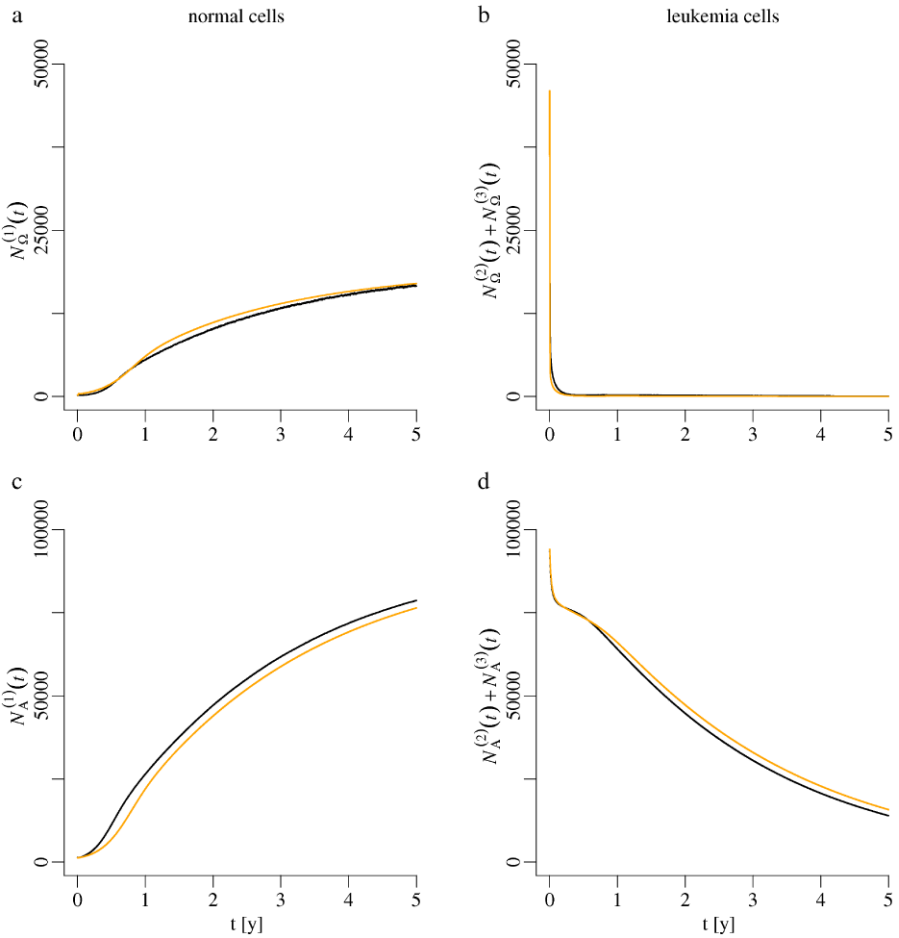

Fig. 5 Cell numbers of normal (cell type "1") and leukemia cells (types "2" and "3"), separated by signaling contexts Ω (above) and A (below), respectively, for IM treatment. The black curves represent averages of 20 ABM simulations, whereas the orange curves depict numerical solutions of the PDE model. (Color figure online.)

sists of more than 99% leukemia stem cells. Furthermore, we let $\tilde{n}_A^{(3)} \equiv 0$ and $\tilde{n}_\Omega^{(3)} \equiv 0$, i.e., at the moment of treatment initiation there are no IM-affected cells.

Leukemia cells (cell type 2) are rendered IM-affected (cell type 3) at a constant rate r_{inh}. As IM is assumed to significantly reduce the proliferation of leukemic cells, we characterize IM-affected cells by an altered weight function $f_\omega^{(3)}$, which is still independent of cell number N_Ω but reduces the transition rate ω considerably (see Suppl. Fig. B.4). As described in Section 2.3, IM is assumed to degrade proliferative leukemia cells, which is modeled by degradation rate r_{deg}. In contrast to the inhibition rate r_{inh}, r_{deg} acts on all leukemia stem cells, i.e., cell types 2 and 3.

Figure 5 and Fig. 6 show the simulation results for IM treatment with respect to cell numbers (Fig. 5) and *BCR-ABL1* transcript levels as defined in (57) (Fig. 6). The black line

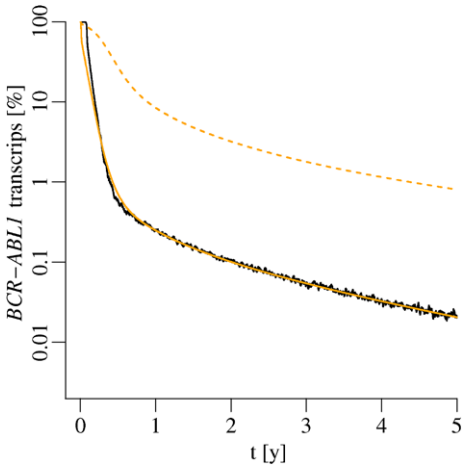

Fig. 6 *BCR-ABL1* transcript levels as defined in (57) for the situation of IM treatment. The black curve depicts the result of the single cell-based model, whereas the orange curves represent solutions of the PDE model (dashed line: original parameter values, solid line: adjusted parameter values as given in the text). (Color figure online.)

corresponds to the single cell-based model, letting $r_{\text{inh}} = 0.05$ and $r_{\text{deg}} = 0.028$. If using exactly the same values for the PDE model, significant quantitative differences between both models can be observed (see dashed line in Fig. 6). Again, this difference might be attributed to the simplified cell cycle structure assumed in the PDE model compared to the ABM. The general qualitative behavior, i.e., the biphasic kinetics, however, is conserved. In order to obtain also a quantitative agreement between both models, it is sufficient to adjust the degradation and inhibition rate. Using $r_{\text{inh}} = 0.19$ and $r_{\text{deg}} = 0.06$, one obtains the results depicted by the solid orange lines, which can be characterized as a very good quantitative agreement between both models.

5. Discussion

We demonstrated in this work that the average dynamic behavior of the previously described ABM of hematopoietic stem cell organization can qualitatively and quantitatively be captured by the proposed PDE model. Even though structural and computational simplifications have been introduced to facilitate an easier numerical handling, all considered scenarios, as there are normal steady-state hematopoiesis, leukemia genesis, and IM treatment dynamics can be reproduced. Beyond this, the PDE model in its presented implementation also qualitatively comprises further situations, such as oscillating cell numbers in the situation of a retarded differentiation process, induced, e.g., by small values of differentiation coefficient d, or system exhaustion for insufficient regenerating capacities, induced, e.g., by small values of regeneration coefficient r and/or high values of d. However, it should be noted that particularly in situations of significant differences in cell numbers (e.g., in oscillating systems), always an individual parameter adjustment of τ_c and κ is required to achieve quantitative consistency, too. The reason for this is mainly

the simplified representation of the cell cycle dynamics in the current implementation of the mean field approach (see also discussion below).

A major advantage of the proposed time-continuous representation is the fact that it is able to efficiently handle systems with huge cell numbers. Therefore, in contrast to the ABM, which requires a down-scaling of stem cell numbers to about $1/10$ of the realistic value in patients to guarantee feasible simulation times, the PDE model allows us to explicitly simulate those systems. This is particularly important because PCR techniques that are applied to monitor the tumor load in terms of the *BCR-ABL1* transcript levels, have an extremely high sensitivity (Hochhaus et al., 2000). They are able to detect about one leukemic cell within 10^5 cells. To be able to describe *BCR-ABL1* levels of less than $10^{-3}\%$, as realistic for residual disease dynamics, ABM simulations become extremely time-consuming. This is particularly the case if one is interested in the average behavior. Due to the stochasticity involved in the ABM, average results require multiple simulation runs, which again considerably increases total simulation times.

To illustrate the differences in the computational costs of the two mathematical approaches (both of which have been implemented in C++) let us consider the three scenarios described in this publication. Using the numerical algorithms outlined in Section 3, it takes approximately 13 minutes to calculate the average population behavior of a normal steady-state system regenerating from only a few cells over a timespan of 3 years (cf. Fig. 3). In contrast, the calculation time of the ABM in the same situation is about 21 minutes, resulting in approximately 7 hours to determine the average of 20 individual simulation runs. For the situation of CML genesis over a timespan of 15 years (cf. Fig. 4) the numerical PDE solution takes about 2.3 hours, in contrast to about 5.3 hours for a single ABM-based simulation. That means, for the determination of an average of 20 simulation runs the PDE approach is about 46-fold faster than the ABM. Similar savings in computation times are also observed for the situation of a 5-year IM treatment (cf. Fig. 6): 1.2 hours in the PDE model compared to 2.1 hours for a single ABM simulation. All simulations have been performed on a LINUX platform using an Intel(R) Xeon(TM) CPU 3.80 GHz with 64 bit architecture and 8 GB RAM. Because the PDE model represents only an approximation of the ABM, the latter should be preferred whenever its calculational costs are not significantly higher compared to the PDE approach.

Despite its advantages, the PDE representation has also a number of limitations. Because it is a mean field approach it does naturally not allow for the description of system immanent heterogeneity, e.g., with respect to differences in the growth kinetics of individual stem cell clones. This makes it difficult to be applied to the situation of coexisting (e.g., treatment-resistant) stem cell clones. Although such clonal differences might be comprised by the introduction of new cell types (each one treated by a separate set of PDEs), it would considerably increase the complexity and, therefore, also the numerical management. A related problem is the fact that small subclones might not be represented correctly in the mean field approach as PDE models are classically derived as the limit of a large number of interacting cells. Hence, the situation of small clone phenomena is not considered in this paper. Furthermore, the PDE model cannot account for effects caused by stochastic fluctuations. One example is clonal extinction in the situation of CML genesis. Whereas the stochastic ABM approach allows for the fact that a small clone might disappear simply due to stochastic fluctuations, even if the clone exhibits a relative growth advantage, the deterministic description would predict an ultimate expansion of any such

newly induced clone. Particularly, only about 20% of induced single-cell mutations representing the generation of the Philadelphia chromosome (see Section 4.2) lead to the formation of a manifest leukemia in the context of the ABM. The remaining 80% of the induced malignant clones become extinct owing to the stochastic fluctuations of clone sizes. Therefore, to allow for a quantitative comparison of ABM and PDE model, the ABM average simulations of CML genesis shown in this publication comprise only the 20% successfully engrafted malignant clones.

Another limitation of the proposed PDE implementation is the simplified representation of cell cycle regulation. As discussed in the results section, this does only incompletely fit the results of the agent-based system and requires the individual adaptation of the model parameters governing $\tau_c(N)$ and $\kappa(N)$. However, as no detailed experimental estimates for parameters underlying the dynamic cell cycle regulation are available, the application of a simplified cell cycle regulation in the PDE model does not represent a general constraint. Alternative simplifications of the model structure, however, will inevitably break the model. Stem cell heterogeneity (as represented by the a-distribution) and proliferative regulation (modeled via the A and Ω signaling contexts) can be considered "core" concepts of the model that should not be changed.

It should be noted at this point that the representation of the stem cell model as a system of PDEs is not the only way to enhance computational efficiency. Kim et al. (2008a) developed a difference equation representation of the stem cell model proposed by our group. This approach also provides an efficient method to simulate CML genesis and treatment, while maintaining the complete structural complexity of the underlying ABM. In another publication, Kim et al. (2008b) developed a PDE representation of our agent-based model, which incorporates the complete structure of the underlying ABM. As a result, the PDE model is rather expensive to solve numerically. We could show in our work that the situation of CML genesis and treatment does not require the full complexity of the ABM and can thus be handled by a computationally less demanding approach compared to the Kim model. Another approach to describe CML dynamics has been proposed by Michor and colleagues (Michor et al., 2005; Dingli and Michor, 2006; Michor, 2007). These authors apply systems of ordinary differential equations. While this is a highly efficient method in terms of computation time, it neglects the heterogeneity of the stem cell compartment, both with respect to cell cycle activity as well as with respect to an "age"-structure of the differentiation state of HSCs. Nevertheless, if parametrized correctly, also these models are suitable to explain the average *BCR-ABL1* dynamics of CML patients treated with IM (Roeder and Glauche, 2007). Colijn and Mackey (2005) presented a differential delay equation model on a periodic variant of CML, where oscillations with respect to cell numbers can be observed at differentiated cell stages (e.g., leukocytes and platelets). In contrast to our work, where a general model of hematopoietic stem cell organization is applied to the situation of CML, the model by Mackey and Colijn is specifically designed for the situation of periodic CML mainly on the level of differentiated cells.

In summary, one can say that the presented PDE approach is an appropriate alternative to the previously proposed ABM to describe normal and malignant hematopoietic stem cell dynamics. Although there are some quantitative discrepancies between these two mathematical descriptions mainly due to differences in the representation of the cell cycle dynamics, the results are structurally identical. The major advantage of the PDE approach lies in a highly efficient determination of the average behavior in systems with huge cell populations.

Acknowledgements

This work has been supported by the German Research Foundation (DFG), grant RO3500/1-1 to I.R.

Appendix A

Table A.1 Parameter values for cell types (1), (2), and (3), denoting normal, leukemia, and IM-affected cells, respectively. Model parameters used in the numerical simulations are $a_{\min}/a_{\max}$: minimum/maximum value of affinity a that characterizes the propensity of a cell to reside in signaling context A; d: differentiation coefficient; r: regeneration coefficient; f_α/f_ω: weight functions included in the calculation of α and ω (as defined in (17) and (18)), which denote the transition rate from Ω to A and from A to Ω, respectively; $f_\alpha(.)/f_\omega(.)$: function value of weight functions at given argument; $\tilde{N}_A/\tilde{N}_\Omega$: scaling factor of weight functions (see definition (19) for details); $\tau_c(N)/\kappa(N)$: cell number-dependent cell cycle duration and G_1-phase proportion, which are uniquely determined by parameters λ_i as given in definition (56); r_{inh}: inhibition rate; r_{deg}: degradation rate. Numbers in brackets denote alternative parameter values, which are explained in the respective results sections. Please note that the values marked with an asterisk are exclusively used in the treatment scenario and are set to zero during leukemia genesis

Parameter	Type (1)	Type (2)	Type (3)
$a_{\min}$	0.002	0.002	0.002
$a_{\max}$	1.0	1.0	1.0
d	1.05	1.05	1.05
r	1.1	1.1	1.1
$f_\alpha(0)$	0.5	1.0	1.0
$f_\alpha(\tilde{N}_A/2)$	0.45	0.9	0.9
$f_\alpha(\tilde{N}_A)$	0.05	0.058	0.058
$f_\alpha(\infty)$	0.0	0.0	0.0
$\tilde{N}_A$	10^5	10^5	10^5
$f_\omega(0)$	0.5	1.0	0.05
$f_\omega(\tilde{N}_\Omega/2)$	0.3	0.99	0.049
$f_\omega(\tilde{N}_\Omega)$	0.1	0.98	0.048
$f_\omega(\infty)$	0.0	0.96	0.046
$\tilde{N}_\Omega$	10^5	10^5	10^5
$\tau_c(N)$			
λ_1	24	24 (19)	19
λ_2	400	400	400
λ_3	$6.6 \cdot 10^{-5}$	$6.6 \cdot 10^{-5}$	$6.6 \cdot 10^{-5}$
λ_4	24 (16)	16	16
$\kappa(N)$			
λ_1	0.36	0.36	0.36
λ_2	1000	1000	1000
λ_3	$8.2 \cdot 10^{-5}$	$8.2 \cdot 10^{-5}$	$8.2 \cdot 10^{-5}$
λ_4	0.26	0.26	0.26
r_{inh}	0.0	0.05* (0.19*)	0.0
r_{deg}	0.0	0.028* (0.06*)	0.028 (0.06)

Appendix B: Supplement figures

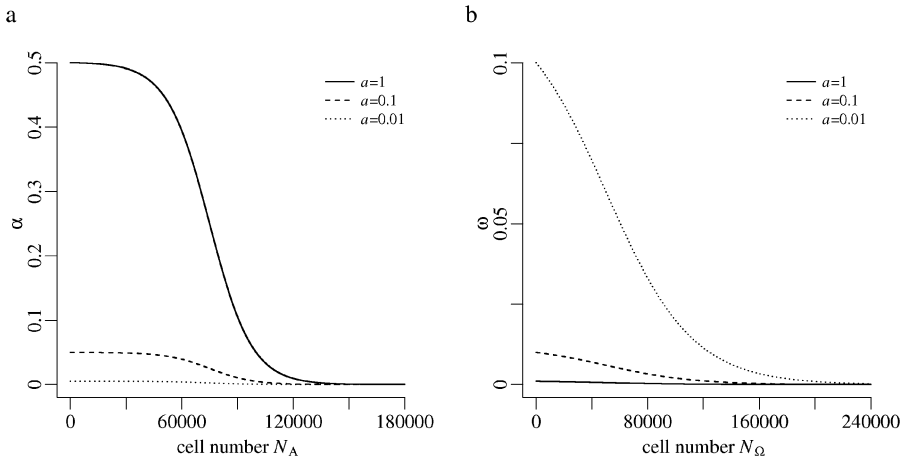

Fig. B.1 Graphical illustration of transition rates α (panel a) and ω (panel b), describing the transition from signaling context Ω to A and from context A to Ω, respectively. The rates depend on the number of cells in the target context, denoted as N_A and N_Ω, and the context affinity a. For instance, cells in Ω with $a = 0.01$ change to A at a negligible rate (dotted line in panel a), whereas cells with $a = 1$, particularly for low cell numbers in context A, change to A at a comparatively high rate (solid line in panel a). For illustrating purposes, we here let $\kappa \equiv 1$.

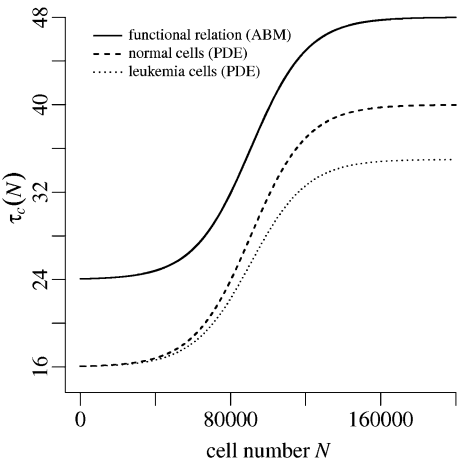

Fig. B.2 Functional relationships of average cell cycle time τ_c and total cell number N used in the model. The solid line corresponds to the empirically determined relationship obtained from the ABM by computer simulation. The dashed line depicts the shifted function used for the simulation of steady-state hematopoiesis, and the dotted line represents the compressed function used for leukemia cells.

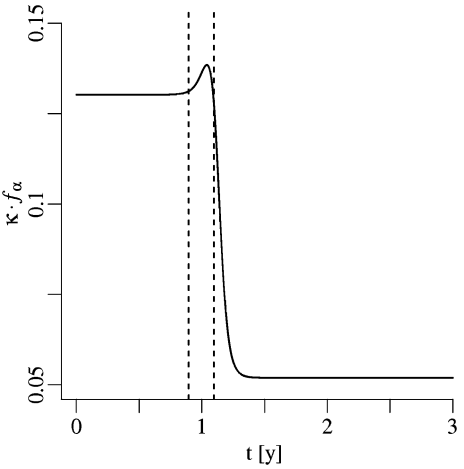

Fig. B.3 Product of κ and f_α functions followed over time to elucidate the transient oscillatory behavior in the PDE solution of the growth phase. Vertical lines represent the corresponding time interval.

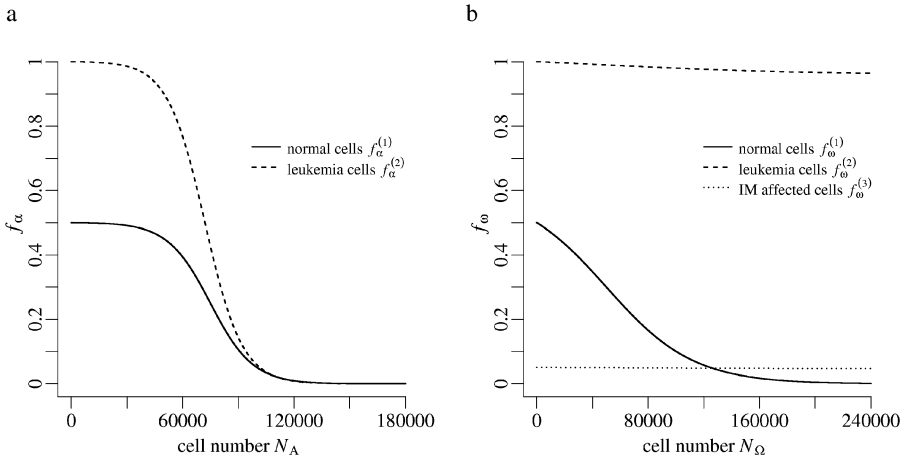

Fig. B.4 Graphical illustration of weight functions f_α and f_ω for cell types (1), (2), and (3).

References

Atkinson, K.A., 1989. An Introduction to Numerical Analysis, 2nd edn. Wiley, New York.

Branford, S., Hughes, T.P., Rudzki, Z., 1999. Monitoring chronic myeloid leukaemia therapy by real-time quantitative PCR in blood is a reliable alternative to bone marrow cytogenetics. Br. J. Haematol. 107(3), 587–599.

Buchdunger, E., Zimmermann, J., Mett, H., Meyer, T., Müller, M., Druker, B.J., Lydon, N.B., 1996. Inhibition of the Abl protein-tyrosine kinase in vitro and in vivo by a 2-phenylaminopyrimidine derivative. Cancer Res. 56(1), 100–104.

Colijn, C., Mackey, M.C., 2005. A mathematical model of hematopoiesis: I. Periodic chronic myelogenous leukemia. J. Theor. Biol. 237(2), 117–132.

Dingli, D., Michor, F., 2006. Successful therapy must eradicate cancer stem cells. Stem Cells 24(12), 2603–2610.
d'Inverno, M., Luck, M., 2004. Understanding Agent Systems, 2nd edn. Springer, Berlin.
Druker, B.J., Tamura, S., Buchdunger, E., Ohno, S., Segal, G.M., Fanning, S., Zimmermann, J., Lydon, N.B., 1996. Effects of a selective inhibitor of the Abl tyrosine kinase on the growth of Bcr-Abl positive cells. Nat. Med. 2(5), 561–566.
Glauche, I., Cross, M., Loeffler, M., Roeder, I., 2007. Lineage specification of hematopoietic stem cells: mathematical modeling and biological implications. Stem Cells 25(7), 1791–1799.
Hochhaus, A., Weisser, A., La Rosée, P., Emig, M., Müller, M.C., Saussele, S., Reiter, A., Kuhn, C., Berger, U., Hehlmann, R., Cross, N.C., 2000. Detection and quantification of residual disease in chronic myelogenous leukemia. Leukemia 14(6), 998–1005.
Holtz, M., Forman, S.J., Bhatia, R., 2007. Growth factor stimulation reduces residual quiescent chronic myelogenous leukemia progenitors remaining after imatinib treatment. Cancer Res. 67(3), 1113–1120.
Horn, M., Loeffler, M., Roeder, I., 2008. Mathematical modeling of genesis and treatment of chronic myeloid leukemia. Cells Tissues Organs 188(1–2), 236–247.
Jørgensen, H.G., Copland, M., Allan, E.K., Jiang, X., Eaves, A., Eaves, C., Holyoake, T., 2006. Intermittent exposure of primitive quiescent chronic myeloid leukemia cells to granulocyte-colony stimulating factor in vitro promotes their elimination by imatinib mesylate. Clin. Cancer Res. 12(2), 626–633.
Kim, P.S., Lee, P.P., Levy, D., 2008a. Modeling imatinib-treated chronic myelogenous leukemia: reducing the complexity of agent-based models. Bull. Math. Biol. 70(3), 728–744.
Kim, P.S., Lee, P.P., Levy, D., 2008b. A PDE model for imatinib-treated chronic myelogenous leukemia. Bull. Math. Biol. doi:10.1007/s11538-008-9336-z.
LeVeque, R.J., 1990. Numerical Methods for Conservation Laws. Birkhäuser, Basel.
Loeffler, M., Roeder, I., 2002. Tissue stem cells: definition, plasticity, heterogeneity, self-organization and models—a conceptual approach. Cells Tissues Organs 171(1), 8–26.
Mauro, M.J., Druker, B.J., 2001. Chronic myelogenous leukemia. Curr. Opin. Oncol. 13(1), 3–7.
Metz, J.A.J., Diekmann, O., 1986. The Dynamics of Physiologically Structured Populations. Springer, Berlin.
Michor, F., 2007. Reply: the long-term response to imatinib treatment of CML. Br. J. Cancer 96(4), 679–680.
Michor, F., Hughes, T.P., Iwasa, Y., Branford, S., Shah, N.P., Sawyers, C.L., Nowak, M.A., 2005. Dynamics of chronic myeloid leukaemia. Nature 435(7046), 1267–1270.
Roeder, I., 2003. Dynamic Modeling of Hematopoietic Stem Cell Organization—Design and Validation of the New Concept of Within-Tissue Plasticity. Dissertation, University of Leipzig, ISSN: 1610-7233.
Roeder, I., Glauche, I., 2007. Pathogenesis, treatment effects, and resistance dynamics in chronic myeloid leukemia—insights from mathematical model analyses. J. Mol. Med. 86(1), 17–27.
Roeder, I., Loeffler, M., 2002. A novel dynamic model of hematopoietic stem cell organization based on the concept of within-tissue plasticity. Exp. Hematol. 30(8), 853–861.
Roeder, I., Lorenz, R., 2006. Asymmetry of stem cell fate and the potential impact of the niche: observations, simulations, and interpretations. Stem Cell Rev. 2(3), 171–180.
Roeder, I., Kamminga, L.M., Braesel, K., Dontje, B., de Haan, G., Loeffler, M., 2005. Competitive clonal hematopoiesis in mouse chimeras explained by a stochastic model of stem cell organization. Blood 105(2), 609–616.
Roeder, I., Horn, M., Glauche, I., Hochhaus, A., Mueller, M.C., Loeffler, M., 2006. Dynamic modeling of imatinib-treated chronic myeloid leukemia: functional insights and clinical implications. Nat. Med. 12(10), 1181–1184.
Roeder, I., Braesel, K., Lorenz, R., Loeffler, M., 2007. Stem cell fate analysis revisited: interpretation of individual clone dynamics in the light of a new paradigm of stem cell organization. J. Biomed. Biotechnol. 2007(3), 84656.
Savage, D.G., Antman, K.H., 2002. Imatinib mesylate—a new oral targeted therapy. N. Engl. J. Med. 346(9), 683–693.
Spanier, J., Oldham, K.B., 1987. The Dirac delta function $\delta(x-a)$. In: An Atlas of Functions, pp. 79–82. Hemisphere, Washington. Chap. 10.
Vigneri, P., Wang, J.Y., 2001. Induction of apoptosis in chronic myelogenous leukaemia cells through nuclear entrapment of BCR-ABL tyrosine kinase. Nat. Med. 7(2), 228–234.